Utah State University

From the SelectedWorks of Bela G. Fejer

November 1, 2004

Average nighttime F region disturbance neutral winds measured by WINDI UARS: Initial results

J. T. Emmert
Bela G. Fejer, *Utah State University*
G. G. Shepard
B. H. Solheim

Available at: https://works.bepress.com/bela_fejer/139/

Average nighttime *F* region disturbance neutral winds measured by UARS WINDII: Initial results

J. T. Emmert
School of Computational Sciences, George Mason University, Fairfax, Virginia, USA

B. G. Fejer
Center for Atmospheric and Space Science, Utah State University, Logan, Utah, USA

G. G. Shepherd and B. H. Solheim
Centre for Research in Earth and Space Science, York University, Toronto, Ontario, Canada

Received 24 September 2004; revised 23 October 2004; accepted 1 November 2004; published 27 November 2004.

[1] We use low- and mid-latitude wind data from the Wind Imaging Interferometer (WINDII) on board the Upper Atmosphere Research Satellite (UARS) to study the average response of nighttime upper thermospheric winds to geomagnetic activity. We calculate perturbation winds in magnetic coordinates and analyze them as a function of magnetic local time, latitude, geomagnetic activity, and solar EUV flux. The nighttime zonal disturbance winds are predominately westward, with the strongest effects extending from dusk at 70° to midnight at 45°. Westward disturbance winds are also observed throughout most of the night at low latitudes, where they change to eastward at dawn. Eastward perturbations occur in the post-midnight sector above 50°. The meridional disturbance winds are primarily equatorward above 40° and after 0300 MLT. In the midnight sector during low and moderate solar flux conditions, poleward winds are observed below 40°; during solar maximum, the perturbations are largely equatorward throughout the night. *INDEX TERMS:* 0358 Atmospheric Composition and Structure: Thermosphere—energy deposition; 2427 Ionosphere: Ionosphere/atmosphere interactions (0335); 3309 Meteorology and Atmospheric Dynamics: Climatology (1620); 3369 Meteorology and Atmospheric Dynamics: Thermospheric dynamics (0358). **Citation:** Emmert, J. T., B. G. Fejer, G. G. Shepherd, and B. H. Solheim (2004), Average nighttime *F* region disturbance neutral winds measured by UARS WINDII: Initial results, *Geophys. Res. Lett.*, *31*, L22807, doi:10.1029/2004GL021611.

1. Introduction

[2] Neutral winds are an important component of the coupled thermosphere-ionosphere system, and understanding their response to geospace storms is necessary to predict changes in the distribution of plasma and other constituents during disturbed conditions. The thermospheric and ionospheric response to magnetic activity has been the subject of numerous case studies [e.g., *Emery et al.*, 1999; *Zhang and Shepherd*, 2002] and numerical simulations [e.g., *Fuller-Rowell et al.*, 2002; *Burns et al.*, 1995]. Relatively few studies, mostly of high-latitude regions, have examined the climatology of storm-time winds [e.g., *Duboin and Lafeuille*, 1992; *Richmond et al.*, 2003]. Recently, data from the Wind Imaging Interferometer (WINDII) on board the Upper Atmosphere Research Satellite (UARS) have been used to study the average response of daytime low- and mid-latitude winds to increased geomagnetic activity [*Fejer et al.*, 2000; *Emmert et al.*, 2001, 2002]. *Fejer et al.* [2002] performed a similar analysis of nighttime winds over the mid-latitude station of Millstone Hill (43°N, 72°W), but the average response of nighttime winds at lower latitudes, or at other longitudes, has not been studied. In this paper, we analyze WINDII data to determine, for the first time, nighttime disturbance neutral wind patterns in the *F* region of the ionosphere at all geomagnetic latitudes below 70°. In the following sections, we describe the WINDII data and outline our procedure for obtaining perturbation winds. Then we present climatological averages of the disturbance winds as a function of magnetic local time and latitude, geomagnetic activity, and solar flux.

2. Data and Methodology

[3] We used upper thermospheric horizontal wind measurements from UARS WINDII. UARS is in a circular, 57° inclination orbit at a height of 585 km; the orbit precesses at a rate of 5° per day. WINDII is a Michelson interferometer that measures Doppler shifts (and hence neutral winds) of the green line (557.7 nm) and red line (630.0 nm) airglow emissions at the Earth's limb, covering latitudes up to 72°. Details of the WINDII instrument, observing geometry, and data sampling characteristics can be found in *Shepherd et al.* [1993] and *Fejer et al.* [2000].

[4] Our previous analyses of WINDII winds utilized the version 4.98 data set, which covered the period November 1991–August 1996. For this study, we used the more extensive version 5.11 data set, which spans November 1991–August 1997 and includes a substantial number of additional data from the 1991–1996 time period. Our present study is focused on nighttime data in the 225–275 km height range (for which only red line data are available), but we also include daytime green and red line data for continuity. Table 1 summarizes the number of wind data contained in the v4.98 and v5.11 data sets. As shown below, the nighttime red line data give results that are consistent with those of the daytime data.

[5] Following the methodology outlined by *Fejer et al.* [2000] and *Emmert et al.* [2001, 2002], we first obtained

Copyright 2004 by the American Geophysical Union.
0094-8276/04/2004GL021611

Table 1. Statistical Characteristics of WINDII 225–275 km Data

	No. of Height Profiles		No. of Days	
	v4.98	v5.11	v4.98	v5.11
Nighttime Red Line	42,300	86,300	85	251
Daytime Red Line	36,600	72,800	87	225
Daytime Green Line	203,400	272,000	502	832

quiet-time reference winds by selecting data for which $Kp < 3$ and averaging in bins of two orbital coordinates: the local time of the ascending node (northward equator crossing), and the argument of latitude (angle from the ascending node). Note that these coordinates have a one-to-one correspondence with geographic local time and latitude. We averaged the data in 1-hour by 10° bins, separating north-looking and south-looking data (the orientation of UARS is reversed every 36 days), red and green line data, and three seasonal bins (Nov–Feb; May–Aug; and Mar, Apr, Sep, Oct). For the daytime red line data, we also treated the 1991–1993 and 1994–1997 observations separately, in order to account for a known offset between these two periods. We repeated this procedure for each height level between 225 and 275 km (the height resolution is 5 km), and then subtracted from each measurement the corresponding quiet-time reference average to obtain a set of residual winds. Quiet-time local time, latitudinal, and seasonal effects were thereby largely removed from the data.

[6] We rotated the residual vector winds into magnetic directions, using Quasi-Dipole (QD) magnetic coordinates and basis vectors [*Richmond*, 1995; *Richmond et al.*, 2003]. To account for quiet-time solar flux effects and for differences between quiet-time patterns in geographic and geomagnetic coordinates, we binned and averaged the quiet-time residuals by emission line (red and green line), QD latitude (5° bins) and local time (1-hour bins), season (same bins as before), and the $F_{10.7}$ proxy for solar EUV flux (3 bins: <100, 100–150, >150). We then applied this new grid of reference averages as a correction to the first set of residuals. Finally, we averaged the residuals over the 225–275 km height range.

[7] The procedure described above is very similar to the one used by *Emmert et al.* [2002] except for the rotation of the residuals into magnetic directions, which allows for easier interpretation of the results in terms of ion-neutral coupling. We use the terms 'perturbations' and 'disturbances' interchangeably to refer to the subset of residuals that correspond to geomagnetically active periods ($Kp \geq 3$). The results described below represent longitudinally averaged conditions in QD coordinates, except that above about 60° some longitude sectors are not sampled. Our results are also seasonally averaged, but the data set is fairly heavily weighted towards December solstice conditions; by combining northern and southern hemispheres, seasonal effects should largely average out. Table 2 summarizes the number of observations and average values in each $F_{10.7}$ and disturbed Kp bin that we used, as well as the distribution of the data by season.

Table 2. Distribution of the v5.11 225–275 km Data Among Several Parameter Bins

	No. of Profiles	Ave. Parameter Value
	Solar Flux	
All	431,100	110
$F_{10.7} \leq 100$	226,800	80
$100 \leq F_{10.7} \leq 150$	141,600	123
$F_{10.7} \geq 150$	62,700	189
	Geomagnetic Activity	
$Kp \geq 3$	165,700	4.0
$3 \leq Kp \leq 4.3$	122,000	3.5
$4 \leq Kp \leq 6$	71,000	4.6
$Kp \geq 5$	29,500	5.6
	Season	
Dec–Feb	209,500	N/A
Mar, Apr, Sep, Oct	156,200	N/A
May–Aug	65,500	N/A

3. Results and Discussion

[8] The WINDII measurements indicate that nighttime mid-latitude zonal disturbance winds are predominately westward, as shown in Figure 1, except above 50°, where there are strong eastward perturbations after 0200 magnetic local time (MLT). Peak westward disturbances occur around 1800 MLT at 60°, but at later times with decreasing latitude; at 20°, the peak occurs near 0300 MLT. The disturbances increase roughly linearly with Kp, as evidenced by the equal spacing of the three curves for different Kp levels. However, above 40° the peak of the westward perturbation shifts to earlier local times with increasing Kp. At 60°, peak westward values range from 120 m/s for $Kp \sim 3.5$ to 240 m/s for $Kp \sim 5.6$, whereas post-midnight eastward disturbances

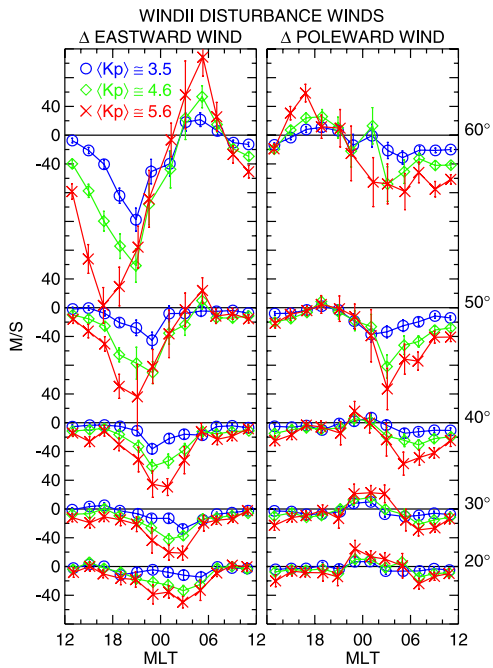

Figure 1. Average mid-latitude disturbance winds as a function of magnetic local time (MLT), with results from three Kp bins superimposed: $3 \leq Kp \leq 4.3$ (blue circles), $4 \leq Kp \leq 6$ (green diamonds), and $Kp \geq 5$ (red crosses). Local time bins are 2 hours wide. Results from different 10° magnetic latitude bins, centered on the indicated values and with northern/southern hemispheres combined, are shown. (left) Zonal component, positive eastward. (right) Meridional component, positive poleward.

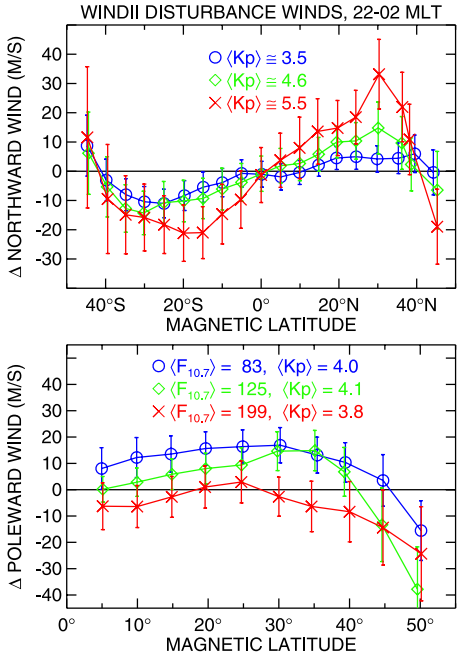

Figure 2. (top) Average low- and mid-latitude meridional disturbance winds in the 2200–0200 MLT sector as a function of magnetic latitude, with results from three *Kp* bins superimposed as in Figure 1. Latitude bins are 10° wide at 5° intervals. (bottom) Same as the top panel, but using a single *Kp* bin ($Kp \geq 3$) and multiple $F_{10.7}$ bins: $F_{10.7} \leq 100$ (blue circles), $100 \leq F_{10.7} \leq 150$ (green diamonds), and $F_{10.7} \geq 150$ (red crosses). Northern/southern hemispheres are combined.

have peak values of 20–120 m/s. The nighttime zonal disturbance winds at 50° and 60° are in good agreement with disturbance winds derived from Millstone Hill (52° magnetic latitude) Fabry-Perot interferometer (FPI) measurements [*Fejer et al.*, 2002]. At 20°, peak westward values range from about 15 to 50 m/s.

[9] The meridional disturbance winds shown in Figure 1 are generally small in the pre-midnight sector and equatorward in the post-midnight sector, with equatorward perturbations appearing at earlier local times with increasing latitude. The largest equatorward values range from 40 m/s for $Kp \sim 3.5$ to 120 m/s for $Kp \sim 5.6$. Poleward disturbances are observed before 1930 MLT at 60° and also around midnight below 50°. In the latter case, the peak values are up to 30 m/s. The meridional perturbations at 50° are in good agreement with the Millstone Hill results of *Fejer et al.* [2002] for high solar EUV conditions, but the WINDII results represent relatively low solar EUV. On the other hand, poleward disturbances are observed in the low-flux Millstone Hill data, but are only seen at lower latitudes in the WINDII data. This apparent discrepancy could be unique to the location of Millstone Hill.

[10] Figure 2 (top) shows that the midnight sector poleward disturbances occur below 40° and peak at 20°–30° with values of 10 m/s (weakly disturbed) to 30 m/s (strongly disturbed). Results are fairly similar in each hemisphere, even though the seasonal distribution is quite different. Figure 2 (bottom) shows results from different $F_{10.7}$ levels. The poleward perturbation is strongest during solar minimum; at solar maximum, this feature disappears almost entirely and the disturbance winds become equatorward at essentially all latitudes. This behavior is consistent with the $F_{10.7}$ dependence of the Millstone Hill FPI disturbance winds [*Fejer et al.*, 2002].

[11] The low-latitude nighttime zonal disturbance winds (Figure 3) are characterized by a westward peak near 0300 MLT and a less distinct, but consistent, westward peak near 1930 MLT. Quiet-time low-latitude winds are predominately eastward at night, so the westward perturbations represent a reduction in wind speed. As *Kp* increases, the post-midnight peak becomes stronger and broadens toward earlier local times. At 10° and below, a west-to-east transition occurs at 0600 MLT. The theoretical simulations of *Fuller-Rowell et al.* [2002] suggest that the westward perturbations in the nighttime equatorial region are due to the inhibition of eastward wind development, caused by a damped pre-reversal enhancement that would otherwise lift the ionosphere and reduce drag on the neutrals. Other possible westward wind sources include Coriolis forcing on the equatorward disturbances [e.g., *Blanc and Richmond*, 1980], coupling with the storm-induced westward ion drifts suggested by the mechanism of *Blanc and Richmond* [1980], and the dusk-midnight westward pressure gradients predicted by *Burns et al.* [1995].

[12] Figure 4 summarizes the behavior of the nighttime and daytime WINDII disturbance winds for $Kp \geq 3$, and shows that results from the northern and southern hemispheres are very similar. To generate these figures, binned averages (2-hour MLT bins at 1-hour intervals and 10° latitude bins at 5° intervals up to 75°) were smoothed via a least squares fit to vector spherical harmonics [e.g., *Hedin et al.*, 1988]. The expansion included terms up to orders 12 in latitude and 3 in local time.

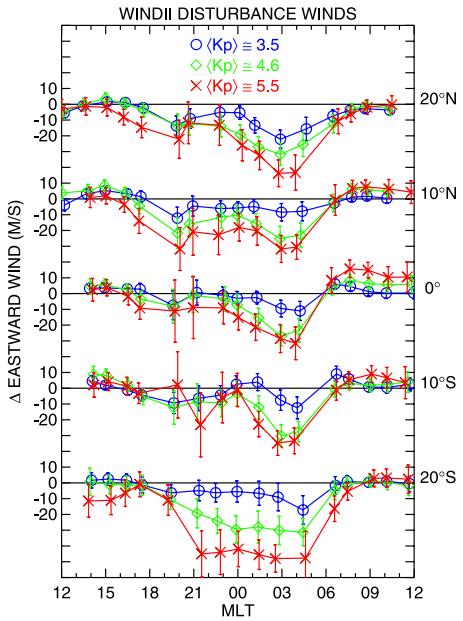

Figure 3. Same as Figure 1, for the zonal component at low latitudes. Local time bins are 3 hours wide at 1.5-hour intervals. Northern/southern hemispheres are averaged separately.

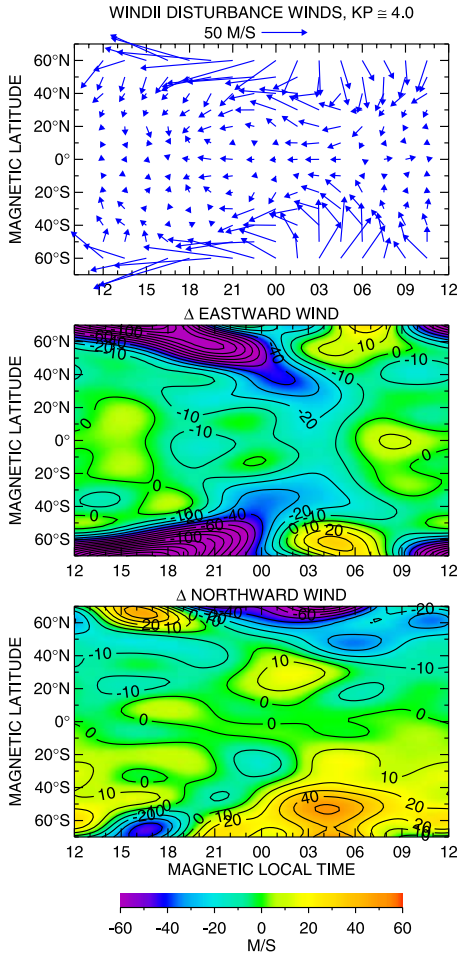

Figure 4. (top) Vector disturbance winds from the empirical model described in the text. (middle and bottom) Zonal and meridional disturbances from the empirical model; the contour interval is 10 m/s.

[13] Figure 4 (top) suggests that the largest equatorward disturbance winds originate at high latitudes (probably as a result of heating-induced pressure gradients) near 0300 MLT and turn westward and then poleward at mid latitudes, possibly as a result of Coriolis forcing. Figure 4 (middle) shows the strong westward perturbations in the dusk sector, with peak values that extend from 70° at 1800 MLT to 45° at midnight. This feature is probably associated with enhanced ion convection. The westward disturbances observed at lower latitudes likely arise from Coriolis and ion drag forces. Figure 4 (bottom) shows the pattern of meridional disturbance winds; the midnight mid-latitude poleward winds (yellow in the northern hemisphere, light blue in the southern) are clearly evident. At high solar activity levels (not shown), these features are displaced by the post-midnight equatorward winds, which become centered on midnight and dominate the pattern.

[14] In summary, the WINDII measurements show that the upper mid-latitude zonal disturbance winds are westward in the dusk sector and change from west to east around 0200 MLT. The location of the peak westward perturbations shifts to lower latitudes with increasing local time. Near the equator, they are predominately westward, shifting to eastward at 0600 MLT. Nighttime meridional disturbances are largely equatorward, except for a region of poleward perturbations observed around midnight below 40° under low and moderate solar activity conditions.

[15] **Acknowledgments.** This material is based on work supported by the National Science Foundation under Grant No. ATM-0407823, and by NASA through grant NAG5-10215. The WINDII project is supported by the Canadian Space Agency and the Centre d'Etudes Spatiales of France. Support for scientific data analysis is provided by the Natural Sciences and Engineering Research Council of Canada.

References

Blanc, M., and A. D. Richmond (1980), The ionospheric disturbance dynamo, *J. Geophys. Res.*, *85*, 1669–1688.

Burns, A. G., T. L. Killeen, W. Deng, G. R. Carignan, and R. G. Roble (1995), Geomagnetic storm effects in the low- to middle-latitude upper thermosphere, *J. Geophys. Res.*, *100*, 14,673–14,692.

Duboin, M.-L., and M. Lafeuille (1992), Thermospheric dynamics above Saint-Santin: Statistical study of the data set, *J. Geophys. Res.*, *97*, 8661–8671.

Emery, B. A., C. Lathuillere, P. G. Richards, R. G. Roble, M. J. Buonsanto, D. J. Knipp, P. Wilkinson, D. P. Sipler, and R. Niciejewski (1999), Time dependent thermospheric neutral response to the 2–11 November 1993 storm period, *J. Atmos. Sol. Terr. Phys.*, *61*, 329–350.

Emmert, J. T., B. G. Fejer, C. G. Fesen, G. G. Shepherd, and B. H. Solheim (2001), Climatology of middle- and low latitude *F* region disturbance neutral winds measured by wind imaging interferometer (WINDII), *J. Geophys. Res.*, *106*, 24,701–24,712.

Emmert, J. T., B. G. Fejer, G. G. Shepherd, and B. H. Solheim (2002), Altitude dependence of mid and low latitude daytime thermospheric disturbance winds measured by WINDII, *J. Geophys. Res.*, *107*(A12), 1483, doi:10.1029/2002JA009646.

Fejer, B. G., J. T. Emmert, G. G. Shepherd, and B. H. Solheim (2000), Average daytime *F* region disturbance neutral winds measured by UARS: Initial results, *Geophys. Res. Lett.*, *27*, 1859–1862.

Fejer, B. G., J. T. Emmert, and D. P. Sipler (2002), Climatology and storm-time dependence of nighttime thermospheric neutral winds over Millstone Hill, *J. Geophys. Res.*, *107*(A5), 1052, doi:10.1029/2001JA000300.

Fuller-Rowell, T. J., G. H. Millward, A. D. Richmond, and M. V. Codrescu (2002), Storm-time changes in the upper atmosphere at low latitudes, *J. Atmos. Sol. Terr. Phys.*, *64*, 1383–1391.

Hedin, A. E., N. W. Spencer, and T. L. Killeen (1988), Empirical global model of upper thermosphere winds based on Atmosphere and Dynamics Explorer satellite data, *J. Geophys. Res.*, *93*, 9959–9978.

Richmond, A. D. (1995), Ionospheric electrodynamics using magnetic apex coordinates, *J. Geomagn. Geoelectr.*, *47*, 191–212.

Richmond, A. D., C. Lathuillere, and S. Vennerstroem (2003), Winds in the high-latitude lower thermosphere: Dependence on the interplanetary magnetic field, *J. Geophys. Res.*, *108*(A2), 1066, doi:10.1029/2002JA009493.

Shepherd, G. G., et al. (1993), WINDII, the Wind Imaging Interferometer on the Upper Atmosphere Research Satellite, *J. Geophys. Res.*, *98*, 10,725–10,750.

Zhang, S. P., and G. G. Shepherd (2002), Neutral winds and O(^{1}S) emission rates in the lower thermosphere as measured with WINDII/UARS during the April 4–5th 1993 and February 1994 geomagnetic storms, *J. Atmos. Sol. Terr. Phys.*, *64*, 1201–1214.

J. T. Emmert, School of Computational Sciences, George Mason University, 4400 University Drive, MS 5C3, Fairfax, VA 22030, USA. (jemmert@gmu.edu)

B. G. Fejer, Center for Atmospheric and Space Science, Utah State University, 4405 Old Main Building, Logan, UT 84322–4405, USA.

G. G. Shepherd and B. H. Solheim, Centre for Research in Earth and Space Science, York University, Toronto, ON, Canada M3J 1P3.